CDDpress

www.nature.com/cddiscovery

ARTICLE OPEN

Check for updates

Functional and developmental changes in the inner hair cell ribbon synapses caused by Myosin VI knockout and deafness-inducing point mutation

Ning Yin[1,2,3,8], Jingjing Zhao[1,2,3,8], Panpan Zhang[4,5,6], Baofu Yu[7], Renjie Chai[4,5,6]✉ and Geng-Lin Li[1,2,3]✉

Hearing loss is one of the most common neurosensory disorders in humans, and above half of hearing loss is caused by gene mutations. Among more than 100 genes that cause non-syndromic hearing loss, myosin VI (MYO6) is typical in terms of the complexity of underlying mechanisms, which are not well understood. In this study, we used both knock-out (*Myo6*$^{-/-}$) and point mutation (*Myo6*^{C442Y}) mice as animal models, performed whole-cell patch-clamp recording and capacitance measurement in the inner hair cells (IHCs) in the cochlea, and sought to reveal potential functional and developmental changes in their ribbon synapses. In *Myo6*$^{-/-}$ cochleae of both before (P8-10) and after hearing onset (P18-20), exocytosis from IHCs, measured in whole-cell capacitance change (ΔC_m), was significantly reduced, Ca^{2+} current amplitude (I_{Ca}) was unchanged, but Ca^{2+} voltage dependency was differently altered, causing significant increase in Ca^{2+} influx in mature IHCs but not in immature IHCs. In immature IHCs of *Myo6*$^{C442Y/C442Y}$ cochleae, neither ΔC_m nor I_{Ca} was altered, but both were reduced in mature IHCs of the same animal model. Furthermore, while the reduction of exocytosis was caused by a combination of the slower rate of depleting readily releasable (RRP) pool of synaptic vesicles and slower sustained release rate (SRR) in *Myo6*$^{-/-}$ immature IHCs, it was likely due to smaller RRP and slower SRR in mature IHCs of both animal models. These results expand our understanding of the mechanisms of deafness caused by MYO6 mutations, and provide a solid theoretical and scientific basis for the diagnosis and treatment of deafness.

Cell Death Discovery (2023)9:177 ; https://doi.org/10.1038/s41420-023-01473-3

INTRODUCTION

Of all the sensory systems in the human body, hearing is the most vulnerable to environmental and genetic factors, resulting in a decline in function or even a complete absence. According to the latest data published on the hereditary hearing loss website, 123 genes are known to have mutations or deletions that can lead to non-syndromic hearing loss [1]. In addition, mutations or deletions of more than 400 genes can lead to syndromic hearing loss [2]. It is worth mentioning that most of these genes contain multiple types of deafness mutations, and the mechanisms of these mutations are not the same [3, 4]. Therefore, although hereditary deafness research has received attention at an early stage, elucidating the deafness mechanism of different deafness genes seems to be a long way to go. Due to the unparalleled structural complexity and functional sophistication of the auditory pathway, especially the cochlea, we can only systematically study different types of mutations in different deafness genes one by one, and there is no shortcut.

Among all the genes that can cause non-syndromic deafness, MYO6 is a very typical representative in terms of the complexity of the deafness mechanism. MYO6 encodes Myosin VI, and the same family contains a large number of genes responsible for different intracellular transport and motor functions, including skeletal muscle contraction [5, 6]. Since the occurrence of hearing in the cochlea relies heavily on the physical property of cells, especially the hair bundles at the top of hair cells are composed mainly of actin, so far at least six members of myosin gene family, including MYO6 are thought to be associated with hearing [3]. Pathogenic variants in the MYO6 gene cause either autosomal dominant inherited non-syndromic hearing loss (DFNA22) or autosomal recessive inherited non-syndromic hearing loss (DFNB37) [7, 8]. MYO6 was first associated with hearing thanks to a new recessive gene mutation found in Jackson's laboratory in the 1960s, which can lead to a serious decline in the hearing and balance perception functions of mice. The gene mutation named Snell's waltzer leads to the deletion of Myosin VI [9]. Roux et al. found that the amplitude of calcium current in IHCs of adult Snell's waltzer mice was not significantly different from that of wild-type mice, but the synaptic vesicle release was remarkably reduced [10]. Strangely, on the same Snell's waltzer

[1]ENT Institute and Department of Otorhinolaryngology, Eye & ENT Hospital, Fudan University, Shanghai 200031, China. [2]NHC Key Laboratory of Hearing Medicine, Fudan University, Shanghai 200031, China. [3]State Key Laboratory of Medical Neurobiology and MOE Frontiers Center for Brain Science, Fudan University, Shanghai 200031, China. [4]State Key Laboratory of Bioelectronics, Department of Otolaryngology Head and Neck Surgery, Zhongda Hospital, School of Life Sciences and Technology, Advanced Institute for Life and Health, Jiangsu Province High-Tech Key Laboratory for Bio-Medical Research, Southeast University, Nanjing 210096, China. [5]Co-Innovation Center of Neuroregeneration, Nantong University, Nantong 226001, China. [6]Department of Otolaryngology Head and Neck Surgery, Sichuan Provincial People's Hospital, University of Electronic Science and Technology of China, Chengdu, China. [7]Department of Plastic and Reconstructive Surgery, Shanghai Ninth People's Hospital Affiliated to Shanghai Jiaotong University School of Medicine, Shanghai 200011, China. [8]These authors contributed equally: Ning Yin, Jingjing Zhao. ✉email: renjiec@seu.edu.cn; genglin.li@fdeent.org

Received: 6 January 2023 Revised: 27 April 2023 Accepted: 16 May 2023
Published online: 31 May 2023

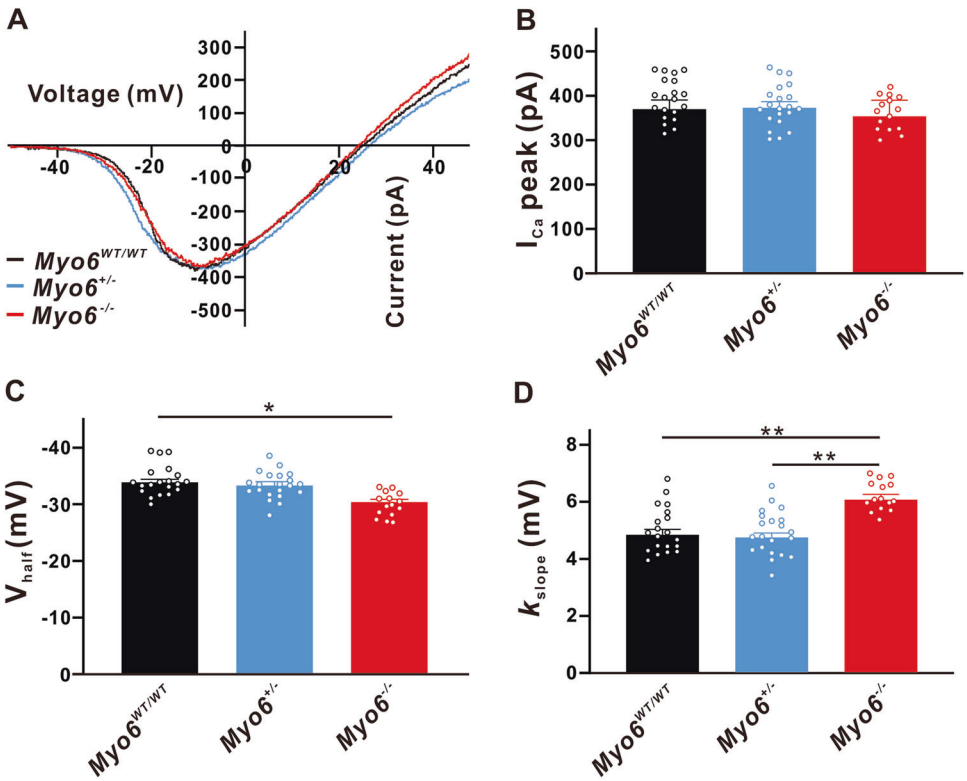

Fig. 1 Properties of I_{Ca} in immature IHCs. A Representative I-V curve of Ca^{2+} currents recorded from $Myo6^{WT/WT}$ mice (black), $Myo6^{+/-}$ mice (blue) and $Myo6^{-/-}$ mice (red) IHCs at P8-10, induced by a voltage ramp from −90 to +70 mV under voltage-clamp and then leak subtracted. **B** The peak amplitude of Ca^{2+} current (I_{Ca}) from three genotypes immature mice IHCs has no significant difference. **C**, **D** I_{Ca} in $Myo6^{-/-}$ mice IHCs has a less negative half-activation voltage (V_{half}) than $Myo6^{WT/WT}$ and a bigger activation slope (k_{slope}) than $Myo6^{WT/WT}$ and $Myo6^{+/-}$. Data are presented as the mean ± SEM. Statistical analysis was by one-way ANOVA. * means $P < 0.05$ and ** means $P < 0.01$.

mice model, another study presented the opposite conclusion: the amplitude of calcium current in IHCs decreased, but there was no significant difference in vesicle release compared with wild-type mice [11]. Therefore, it is necessary to systematically and carefully analyze the functional changes of synaptic transmission of IHCs on different MYO6 mutation mice models in order to fully and deeply reveal the deafness mechanism of Myosin VI gene mutation.

The MYO6 p.C442Y mutation causes DFNA22. Carriers of the MYO6 p.C442Y mutation begin to develop progressive hearing loss during childhood and show profound sensorineural hearing loss by middle age [7]. $Myo6^{C442Y}$ mutation mice with a semidominant inheritance pattern exhibits hearing loss starting from 3 weeks after birth and progresses to severe deafness accompanied by degeneration of hair cells and disorganization of the stereocilia in the organ of Corti [12].

In this study, we used $Myo6^{C442Y}$ point mutation mice and MYO6 knock-out mice as experimental animals, combined with molecular biology and whole-cell patch clamp technology to explore the physiological and pathological mechanisms of MYO6 gene mutation or deletion on auditory development and mutation-induced deafness, thus providing a certain experimental basis for improving and treating non-syndromic deafness.

RESULTS

Effects of MYO6 knock-out on synaptic transmission in developing mice IHCs

We studied synaptic transmission in IHCs of MYO6 knock-out developing mice using whole-cell patch-clamp recordings. IHCs depolarization leads to Ca^{2+} entry, triggering an increase in the overall Ca^{2+} inflow and instantaneous Cm increments, which is controlled by activation of the voltage-dependent Ca^{2+} current.

Three groups of wild ($Myo6^{WT/WT}$), heterozygous ($Myo6^{+/-}$) and homozygous ($Myo6^{-/-}$) mice for experiments to analyze the genetic characteristics of different functional indicators. The acutely isolated mice basement membranes were infiltrated in the external fluid of calcium currents. IHCs were hold at −90 mV and then applied a slow-rising ramp voltage stimulation from −90 mV to +70 mV to induce whole-cell calcium currents at different voltages, and further analyzing the calcium currents at different voltages can obtain the I-V curve (Fig. 1A). We found that there was no significant difference in the peak amplitude of I_{Ca} in IHCs from three genotypes developing mice ($Myo6^{WT/WT}$: 369.5 ± 20.89 pA, $n = 20$; $Myo6^{+/-}$: 372.9 ± 13.86 pA, $n = 21$, $P > 0.05$ vs. $Myo6^{WT/WT}$; $Myo6^{-/-}$: 353.5 ± 36.48 pA, $n = 15$, $P > 0.05$ vs. $Myo6^{WT/WT}$) (Fig. 1B). Then we use Boltzmann function fitting the current-voltage curve to obtain V_{half} and k, which depict the steepness of voltage dependence in Ca^{2+} channels activation in order to characterize the functional properties of IHCs from the three different genotypes mice more comprehensively. V_{half} describes the membrane potential where the conductance is half activated, while k reveals the voltage sensitivity of the activation. Noticing I_{Ca} in $Myo6^{-/-}$ mice has a less negative V_{half} than $Myo6^{WT/WT}$ ($Myo6^{WT/WT}$: −33.89 ± 0.524 mV, $n = 20$; $Myo6^{-/-}$: −30.39 ± 0.5002 mV, $n = 15$, $P < 0.05$) and a bigger activation slope (k_{slope}) than $Myo6^{WT/WT}$ and $Myo6^{+/-}$ ($Myo6^{WT/WT}$: 4.817 ± 0.1977 mV, $n = 20$; $Myo6^{+/-}$: 4.726 ± 0.1597 mV, $n = 21$; $Myo6^{-/-}$: 6.050 ± 0.185 mV, $n = 15$, $P < 0.01$ vs. $Myo6^{WT/WT}$ and $Myo6^{+/-}$) (Fig. 1C, D).

Exocytosis results in incorporation of the membrane from synaptic vesicles into the cell membrane and therefore increases the cell membrane, which can be measured through whole-cell capacitance measurement [13]. Therefore, while recording the voltage-gated calcium current, whole-cell membrane capacitance change (ΔC_m) was monitored to quantify the synaptic vesicle release of IHCs. Figure 2A

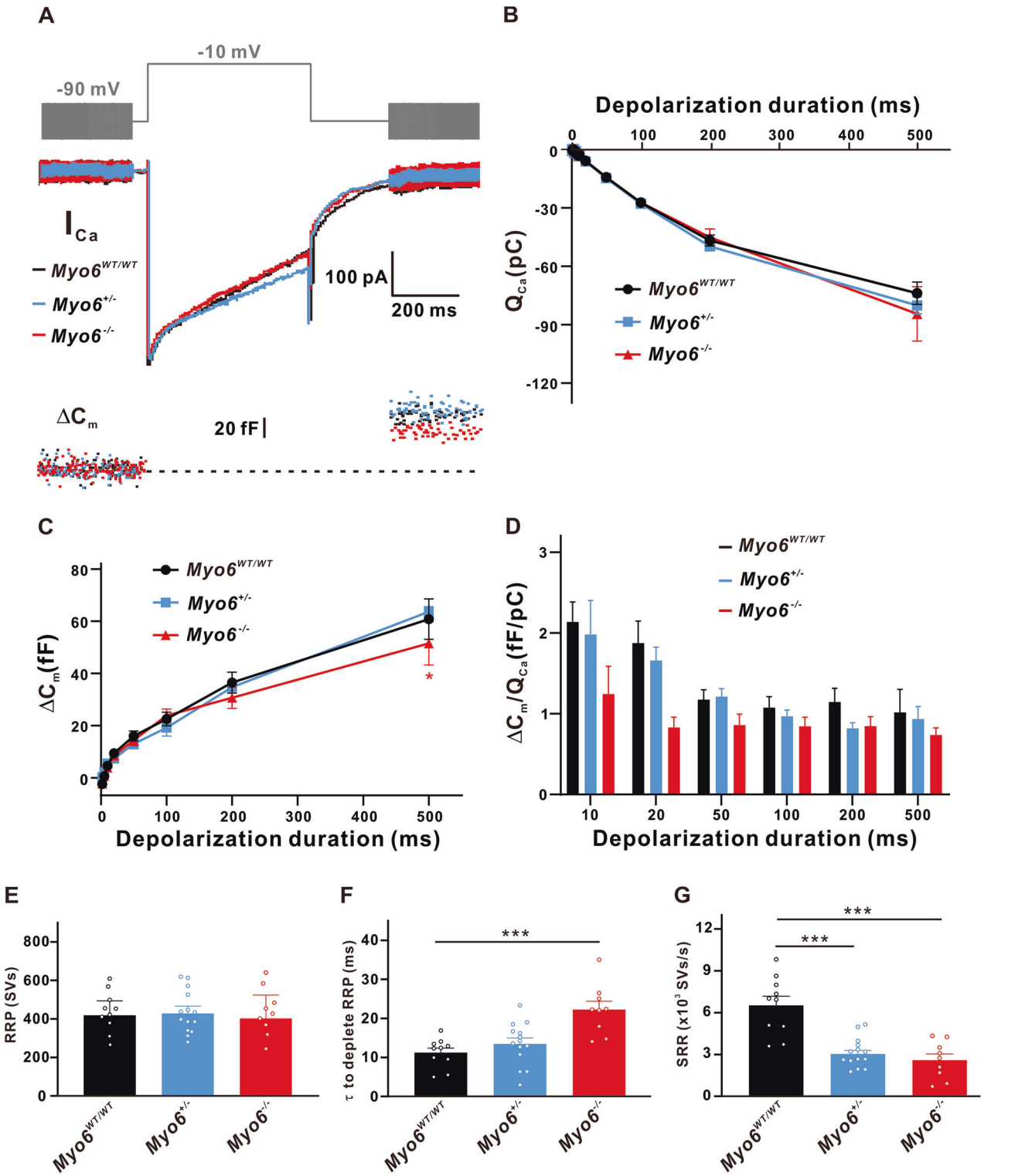

Fig. 2 Exocytosis from immature IHCs. A A representative diagram of I_{Ca} and the corresponding ΔC_m in *Myo6*$^{WT/WT}$ mice (black), *Myo6*$^{+/-}$ mice (blue) and *Myo6*$^{-/-}$ mice (red) IHCs at P8-10 of stimulation duration 500 ms. **B**–**D** Ca^{2+} influx (Q_{Ca}) (**B**) and Ca^{2+} efficiency in triggering exocytosis, the ratio of $\Delta C_m/Q_{Ca}$ (**D**) recorded from three genotypes immature mice IHCs in response to increasing stimulation durations from 2 ms to 500 ms both have no apparent change, but the $\Delta C_{m\ (C)}$ in *Myo6*$^{-/-}$ mice IHCs is remarkably smaller than that in *Myo6*$^{WT/WT}$ mice for duration 500 ms. **E** There was no obvious difference in the readily releasable pool (RRP) of synaptic vesicles. **F** The time constants (τ) to deplete RRP from *Myo6*$^{-/-}$ mice IHCs was significantly longer than that from *Myo6*$^{WT/WT}$ mice IHCs. **G** Sustained release rate (SRR) of synaptic vesicles from *Myo6*$^{-/-}$ mice and *Myo6*$^{+/-}$ mice IHCs was significantly slower than that from *Myo6*$^{WT/WT}$ mice IHCs. Data are presented as the mean ± SEM. Statistical analysis was by one-way or two-way ANOVA. * means $P < 0.05$ and *** means $P < 0.001$.

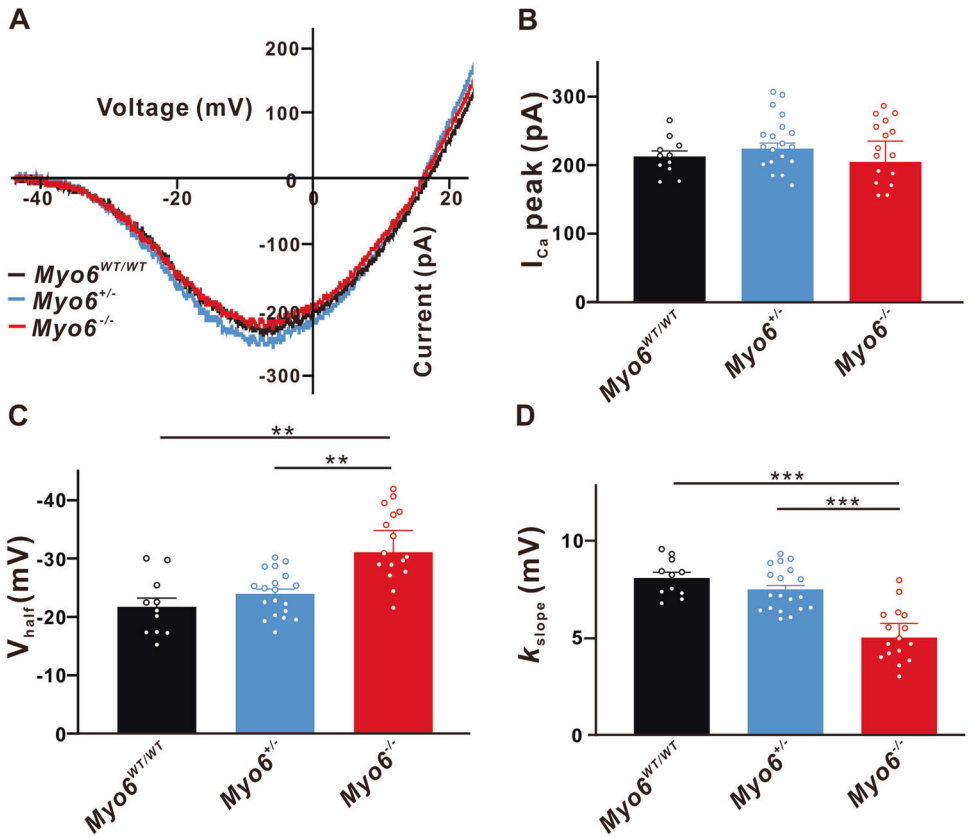

Fig. 3 Properties of I_{Ca} in mature IHCs. A Representative I-V curve of Ca^{2+} currents recorded from $Myo6^{WT/WT}$ mice (black), $Myo6^{+/-}$ mice (blue) and $Myo6^{-/-}$ mice (red) IHCs at P18-20. **B** The peak amplitude of Ca^{2+} current (I_{Ca}) from three genotypes mature mice IHCs has no significant difference. **C**, **D** I_{Ca} in $Myo6^{-/-}$ mice has a more negative half-activation voltage (V_{half}) and a steeper activation slope (k_{slope}) than $Myo6^{WT/WT}$ and $Myo6^{+/-}$. Data are presented as the mean ± SEM. Statistical analysis was by one-way ANOVA. ** means $P < 0.01$ and *** means $P < 0.001$.

shows a representative diagram of I_{Ca} and the corresponding ΔC_m in $Myo6^{WT/WT}$, $Myo6^{+/-}$ and $Myo6^{-/-}$ developing mice IHCs of duration 500 ms. We found that there was no significant difference of Ca^{2+} influx (Q_{Ca}) in IHCs from the three genotypes developing mice when pooled data for Ca^{2+} charge over all stimulation durations were evaluated ($n = 10$ in three groups, $P > 0.05$, Fig. 2B). Additionally, IHCs from $Myo6^{-/-}$ (51.54 ± 8.258 fF, $n = 10$) released fewer synaptic vesicles for long stimulation compared with the $Myo6^{WT/WT}$ (60.82 ± 7.798 fF, $n = 10$, $P < 0.05$; Fig. 2C). However, no observable difference was found in the Ca^{2+} efficiency of exocytosis (qualitatively defined as ΔC_m /Q_{Ca}) for any three groups comparison of the mean values in response to all stimulations from 2 to 500 ms (Fig. 2D), suggesting that Ca^{2+} influx had similar efficiency in triggering $Myo6^{WT/WT}$, $Myo6^{+/-}$ and $Myo6^{-/-}$ mice IHCs exocytosis.

Then we traced vesicles release through capacitance changes and identified two dynamic components of the vesicle pool. The initial small component of ΔC_m increases in response to a short stimulation, representing exocytosis of the RRP of synaptic vesicles located in the active region. Immediately afterward, ΔC_m continues to improve at a slower rate during the stimulation duration of up to 500 ms, indicating vesicles are released from the refilling-pool located farther away from the Ca^{2+} channel. Further analysis showed that the MYO6 knock-out had no effects on the RRP ($Myo6^{WT/WT}$: 418.7 ± 74.99 SVs, $n = 10$; $Myo6^{+/-}$: 428.3 ± 37.83 SVs, $n = 14$; $Myo6^{-/-}$: 402.7 ± 120.9 mV, $n = 9$; $P > 0.05$), but obviously increased the time constants (τ) to deplete RRP ($Myo6^{WT/WT}$: 11.23 ± 1.185 ms, $n = 10$; $Myo6^{+/-}$: 13.50 ± 1.471 ms, $n = 14$; $Myo6^{-/-}$: 22.24 ± 2.144 ms, $n = 9$, $P < 0.001$ vs. $Myo6^{WT/WT}$) and effectively suppressed the sustained release rate (SRR) ($Myo6^{WT/WT}$: 6 517 ± 1 263 SVs/s, $n = 10$; $Myo6^{+/-}$: 3 041 ± 250.1 SVs/s, $n = 14$, $P < 0.001$ vs. $Myo6^{WT/WT}$; $Myo6^{-/-}$: 2 596 ± 642.5 SVs/s, $n = 9$, $P < 0.001$ vs. $Myo6^{WT/WT}$) (Fig. 2E–G), suggesting that MYO6 knock-out developing mice replenish synaptic vesicles less efficiently.

Effects of MYO6 knock-out on synaptic transmission in mature mice IHCs

We selected three groups of mature mice, $Myo6^{WT/WT}$, $Myo6^{+/-}$ and $Myo6^{-/-}$ to record the Ca^{2+} currents of IHCs. Figure 3A shows that the I-V curve of Ca^{2+} currents was obtained. We found that the peak amplitude of I_{Ca} in IHCs from $Myo6^{+/-}$ (224.0 ± 8.070 pA, $n = 19$, $P > 0.05$) and $Myo6^{-/-}$ mice (204.6 ± 30.43 pA, $n = 16$, $P > 0.05$) has no significant change compared with that of $Myo6^{WT/WT}$ mice (212.5 ± 8.116 pA, $n = 11$) (Fig. 3B). Figure 3C, D show that I_{Ca} in $Myo6^{-/-}$ mice IHCs has a more negative V_{half} (−31.11 ± 3.688 mV, $n = 16$, $P < 0.01$ vs. $Myo6^{WT/WT}$ and $Myo6^{+/-}$) and a steeper activation slope (5.016 ± 0.7266 mV, $n = 16$, $P < 0.001$ vs. $Myo6^{WT/WT}$ and $Myo6^{+/-}$) than $Myo6^{WT/WT}$ (V_{half}: −21.71 ± 1.513 mV, $n = 11$; k_{slope}: 8.091 ± 0.2885 mV, $n = 11$) and $Myo6^{+/-}$ (V_{half}: −24.00 ± 0.7672 mV, $n = 19$; k_{slope}: 7.504 ± 0.1932 mV, $n = 19$), revealing that under physiological conditions calcium channels may cause more Ca^{2+} to flow into the IHCs of $Myo6^{-/-}$ mice.

A representative diagram of I_{Ca} and the corresponding ΔC_m in $Myo6^{WT/WT}$, $Myo6^{+/-}$ and $Myo6^{-/-}$ mature mice IHCs of duration 500 ms is shown in Fig. 4A. Further research showed more Ca^{2+} influx (Q_{Ca}) in IHCs from $Myo6^{+/-}$ and $Myo6^{-/-}$ mice ($n = 12$ in three groups, $P < 0.05 \sim 0.01$ vs. $Myo6^{WT/WT}$) (Fig. 4B). Moreover, IHCs from $Myo6^{-/-}$ mice (64.94 ± 6.344 fF, $n = 12$) released fewer

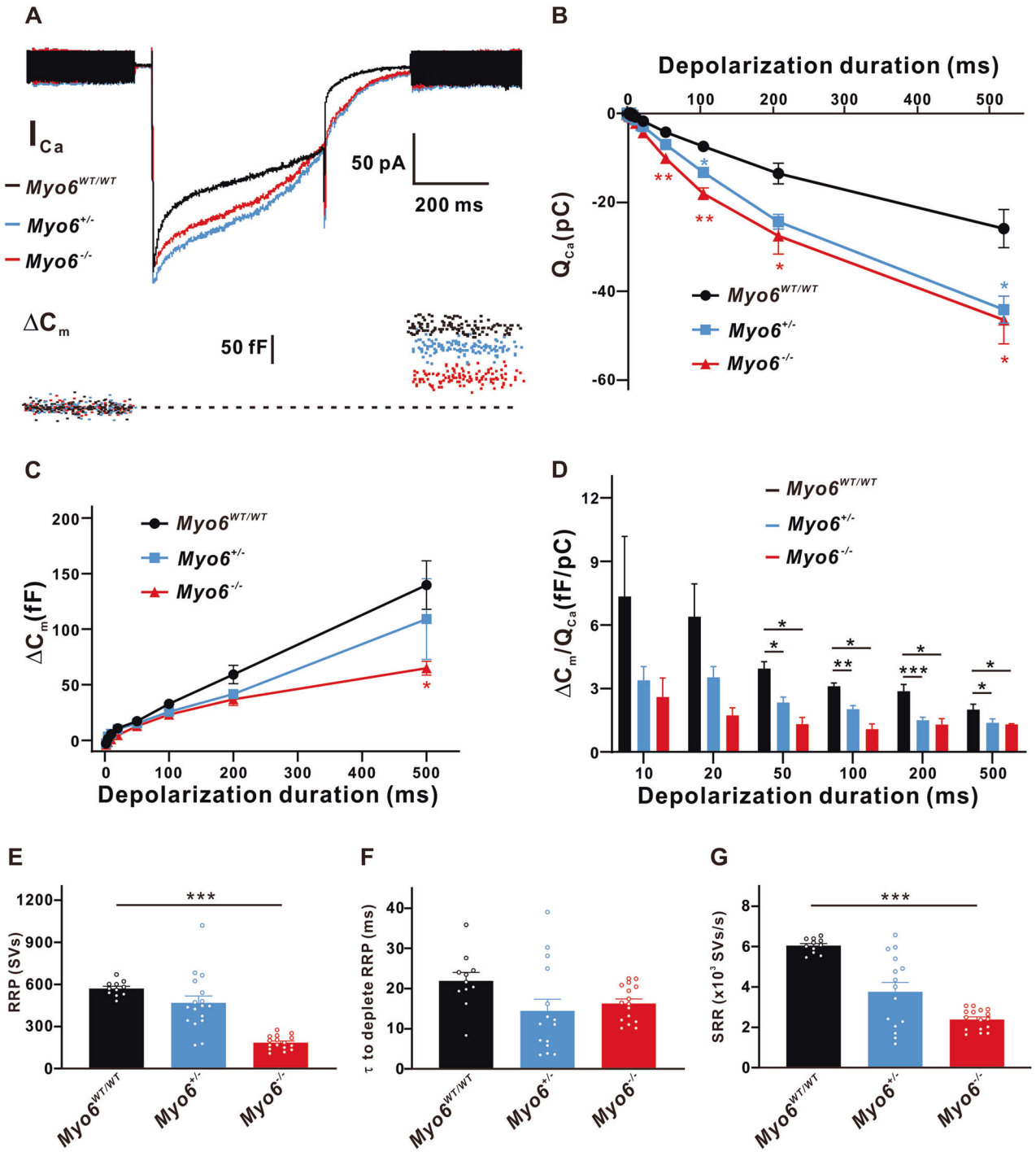

Fig. 4 Exocytosis from mature IHCs. A A representative diagram of I_{Ca} and the corresponding ΔC_m in *Myo6*$^{WT/WT}$ mice (black), *Myo6*$^{+/-}$ mice (blue) and *Myo6*$^{-/-}$ mice (red) IHCs at P18-20 of stimulation duration 500 ms. **B**–**D** Q_{Ca} (**B**) and the ratio of $\Delta C_m/Q_{Ca}$ (**D**) recorded from *Myo6*$^{+/-}$ and *Myo6*$^{-/-}$ mice IHCs have significant difference than that of *Myo6*$^{WT/WT}$ mice for both short and long stimulation, and the ΔC_m (C) in *Myo6*$^{-/-}$ mice IHCs is remarkably smaller than that in *Myo6*$^{WT/WT}$ mice for duration 500 ms. **E** RRP from *Myo6*$^{-/-}$ mice IHCs was prominently smaller than that from *Myo6*$^{WT/WT}$ mice IHCs. **F** There is no obvious difference inτto deplete RRP from three genotypes mature mice. **G** SRR of synaptic vesicles from *Myo6*$^{-/-}$ mice IHCs was significantly slower than that from *Myo6*$^{WT/WT}$ mice IHCs. Data are presented as the mean ± SEM. Statistical analysis was by one-way or two-way ANOVA. * means $P < 0.05$, ** means $P < 0.01$ and *** means $P < 0.001$.

synaptic vesicles for 500 ms stimulation compared with the *Myo6*$^{WT/WT}$ (139.7 ± 21.88 fF, $n = 12$, $P < 0.05$; Fig. 4C). Figure 4D manifests the value of $\Delta C_m/Q_{Ca}$ in *Myo6*$^{+/-}$ and *Myo6*$^{-/-}$ mice IHCs is less than that of *Myo6*$^{WT/WT}$ mice for both short and long stimulation ($n = 12$ in three groups, $P < 0.05 \sim 0.001$), indicating that the Ca^{2+} efficiency of triggering synaptic vesicles release in mature MYO6 knock-out mice was lower than that in wild-type mice. Then we observed that the RRP and SRR in IHCs from *Myo6*$^{-/-}$ mice both prominently smaller than that in IHCs from *Myo6*$^{WT/WT}$ mice (RRP: 570.7 ± 15.78 SVs of *Myo6*$^{WT/WT}$ mice, $n = 11$; 184.4 ± 12.30 SVs of *Myo6*$^{-/-}$ mice, $n = 16$, $P < 0.001$; SRR: 6 046 ± 291.4 SVs/s of *Myo6*$^{WT/WT}$ mice, $n = 11$; 2 387 ± 255.9 SVs/s of *Myo6*$^{-/-}$ mice,

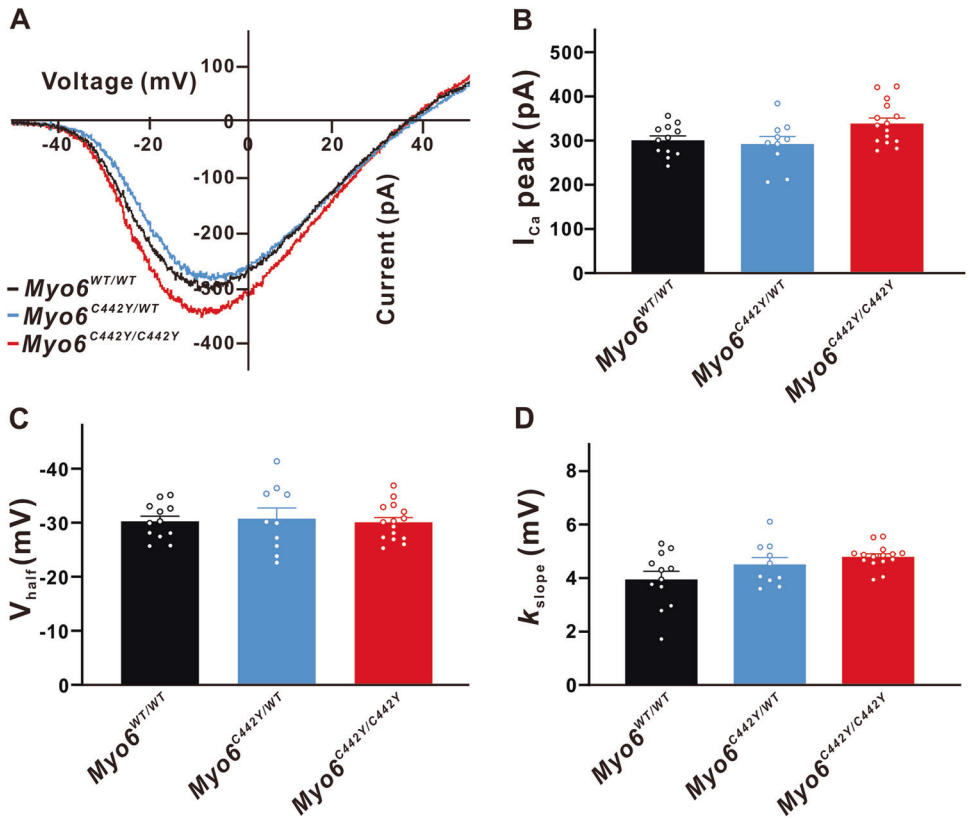

Fig. 5 Properties of I_{Ca} in developing IHCs. A Representative I-V curve of Ca^{2+} currents recorded from $Myo6^{WT/WT}$ mice (black), $Myo6^{C442Y/WT}$ mice (blue) and $Myo6^{C442Y/C442Y}$ mice (red) IHCs at P8-10. **B**–**D** I_{Ca} (**B**), V_{half} (**C**) and k_{slope} (**D**) from three genotypes developing mice IHCs have no distinct difference. Data are presented as the mean ± SEM. Statistical analysis was by one-way ANOVA. $P > 0.05$.

$n = 16$, $P < 0.001$), suggesting that MYO6 knock-out mature mice have a smaller readily releasable pool of synaptic vesicles and replenish synaptic vesicles less efficiently which manifesting its poor function of exocytosis (Fig. 4E, G).

Effects of $Myo6^{C442Y}$ point mutation on synaptic transmission in developing mice IHCs

Three groups of wild ($Myo6^{WT/WT}$), heterozygous ($Myo6^{C442Y/WT}$) and homozygous ($Myo6^{C442Y/C442Y}$) mice were selected for experiments to analyze the genetic characteristics of different functional indicators. We first investigated developing mice.

$Myo6^{C442Y}$ point mutation had no obvious effects on the Ca^{2+} currents amplitude ($Myo6^{WT/WT}$: 300.5 ± 25.32 pA, $n = 12$; $Myo6^{C442Y/WT}$: 292.2 ± 26.59 pA, $n = 10$, $P > 0.05$ vs. $Myo6^{WT/WT}$; $Myo6^{C442Y/C442Y}$: 338.7 ± 24.37 pA, $n = 15$, $P > 0.05$ vs. $Myo6^{WT/WT}$), V_{half} ($Myo6^{WT/WT}$: -30.26 ± 2.337 mV, $n = 12$; $Myo6^{C442Y/WT}$: -30.79 ± 2.455 mV, $n = 10$, $P > 0.05$ vs. $Myo6^{WT/WT}$; $Myo6^{C442Y/C442Y}$: -30.09 ± 2.250 mV, $n = 15$, $P > 0.05$ vs. $Myo6^{WT/WT}$) and slope factor (k_{slope}) of IHCs ($Myo6^{WT/WT}$: 3.951 ± 0.4046 mV, $n = 12$; $Myo6^{C442Y/WT}$: 4.512 ± 0.4249 mV, $n = 10$, $P > 0.05$ vs. $Myo6^{WT/WT}$; $Myo6^{C442Y/C442Y}$: 4.797 ± 0.3895 mV, $n = 15$, $P > 0.05$ vs. $Myo6^{WT/WT}$) (Fig. 5A–D).

And under our experimental conditions we found that the Ca^{2+}-induced exocytosis of IHCs in the developing mice was also not affected by the $Myo6^{C442Y}$ point mutation, ΔC_m ($n = 10$ in three groups, $P > 0.05$ vs. $Myo6^{WT/WT}$), RRP ($Myo6^{WT/WT}$: 337.8 ± 56.66 SVs, $n = 12$; $Myo6^{C442Y/WT}$: 312.5 ± 32.50 SVs, $n = 14$, $P > 0.05$ vs. $Myo6^{WT/WT}$; $Myo6^{C442Y/C442Y}$: 327.0 ± 25.88 SVs, $n = 15$, $P > 0.05$ vs. $Myo6^{WT/WT}$), SRR ($Myo6^{WT/WT}$: 2 961 ± 176.3 SVs/s, n = 12; $Myo6^{C442Y/WT}$: 2 894 ± 410.7 SVs/s, $n = 14$, $P > 0.05$ vs. $Myo6^{WT/WT}$; $Myo6^{C442Y/C442Y}$: 2 755 ± 148.1 SVs/s, $n = 15$, $P > 0.05$ vs. $Myo6^{WT/WT}$), and τ to deplete RRP ($Myo6^{WT/WT}$: 17.73 ± 3.389 ms, $n = 12$; $Myo6^{C442Y/WT}$:16.82 ± 3.866 ms, $n = 14$, $P > 0.05$ vs. $Myo6^{WT/WT}$; $Myo6^{C442Y/C442Y}$: 17.56 ± 5.322 ms, $n = 15$, $P > 0.05$ *vs.* $Myo6^{WT/WT}$) (Fig. 6A–E).

Effects of $Myo6^{C442Y}$ point mutation on synaptic transmission in mature mice IHCs

Moreover, $Myo6^{WT/WT}$, $Myo6^{C442Y/WT}$ and $Myo6^{C442Y/C442Y}$ mature mice were selected to improve our research. We found that the $Myo6^{C442Y}$ mutation resulted in a decrease in I_{Ca} amplitude of IHCs ($Myo6^{WT/WT}$: 229.2 ± 18.65 pA, $n = 12$; $Myo6^{C442Y/WT}$:169.0 ± 20.45 pA, $n = 11$, $P < 0.01$ vs. $Myo6^{WT/WT}$; $Myo6^{C442Y/C442Y}$: 168.1 ± 20.40 pA, $n = 12$; $P < 0.05$ vs. $Myo6^{WT/WT}$) (Fig. 7A, B). But there was no obviously difference in V_{half} of I_{Ca} ($Myo6^{WT/WT}$: -20.96 ± 1.702 mV, $n = 12$; $Myo6^{C442Y/WT}$: −19.56 ± 1.903 mV, $n = 11$, $P > 0.05$ vs. $Myo6^{WT/WT}$; $Myo6^{C442Y/C442Y}$: -23.83 ± 1.903 mV, $n = 12$, $P > 0.05$ vs. $Myo6^{WT/WT}$) (Fig. 7C). Figure 7D testifies to the slope factor of $Myo6^{C442Y/C442Y}$ mice IHCs (8.410 ± 0.201 mV, $n = 12$) is bigger than that of $Myo6^{WT/WT}$ (7.572 ± 0.213 mV, $n = 12$; $P < 0.01$), indicative of less Ca^{2+} influx the IHCs of $Myo6^{C442Y}$ point mutation mice induced by Ca^{2+} channels.

Then we varied stimulation duration from 2 to 500 ms, founding less Q_{Ca} in IHCs from $Myo6^{C442Y/WT}$ and $Myo6^{C442Y/C442Y}$ mice ($n = 12$ in three groups, $P < 0.01$ vs. $Myo6^{WT/WT}$) (Fig. 8B). Giving 500 ms stimulation, the induced ΔC_m of $Myo6^{C442Y/C442Y}$ mice (47.90 ± 10.96 fF, $n = 12$) was remarkably less than that of $Myo6^{WT/WT}$ mice (82.95 ± 10.45 fF, $n = 12$, $P < 0.01$) and $Myo6^{C442Y/WT}$ mice (85.4 ± 10.96 fF, $n = 12$, $P < 0.01$) (Fig. 8C). And the Ca^{2+} efficiency of triggering synaptic vesicles release in mature $Myo6^{C442Y/C442Y}$ mice (0.899 ± 0.151, $n = 12$) was lower than that in $Myo6^{C442Y/WT}$ mice (1.172 ± 0.26, $n = 12$, $P < 0.05$) and $Myo6^{WT/WT}$ mice (1.636 ± 0.299, $n = 12$, $P < 0.05$) (Fig. 8D). Figure 8E, G show that the RRP and SRR in IHCs from $Myo6^{C442Y/C442Y}$ mice both obviously

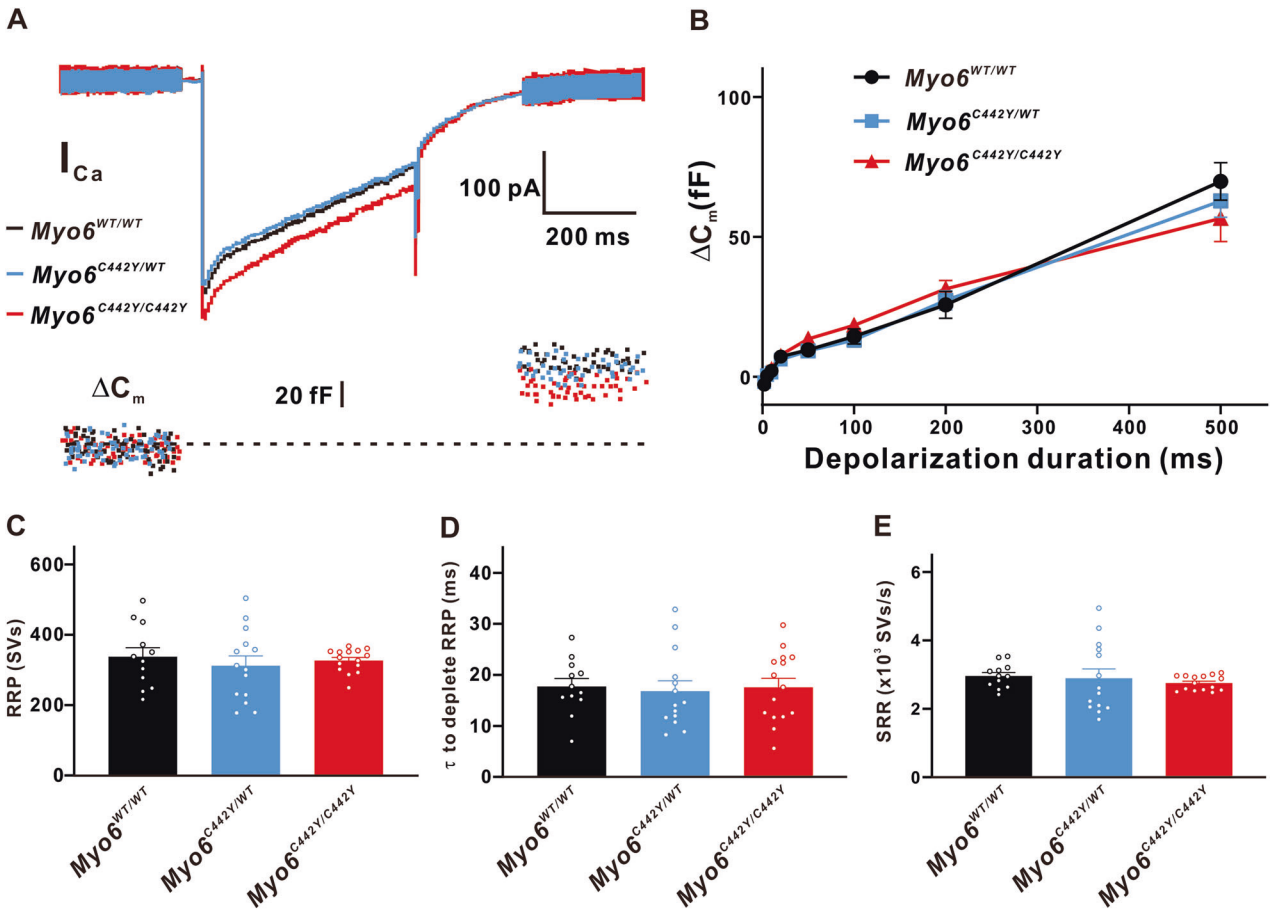

Fig. 6 Exocytosis from developing IHCs. A A representative diagram of I_{Ca} and the corresponding ΔC_m in $Myo6^{WT/WT}$ mice (black), $Myo6^{C442Y/WT}$ mice (blue) and $Myo6^{C442Y/C442Y}$ mice (red) IHCs at P8-10 of stimulation duration 500 ms. **B**–**E** $\Delta C_{m\ (B)}$, RRP (**C**), τ to deplete RRP (**D**) and SRR (**E**) in $Myo6^{C442Y}$ point mutation mice IHCs have no remarkable change than that in $Myo6^{WT/WT}$ mice under physiological conditions. Data are presented as the mean ± SEM. Statistical analysis was by one-way or two-way ANOVA. $P > 0.05$.

decrease than that in IHCs from $Myo6^{WT/WT}$ mice (RRP: 568.4 ± 56.23 SVs of $Myo6^{WT/WT}$ mice, $n = 12$; 366.4 ± 36.29 SVs of $Myo6^{C442Y/C442Y}$ mice, $n = 12$, $P < 0.05$; SRR: 2 691 ± 332.1 SVs/s of $Myo6^{WT/WT}$ mice, $n = 12$; 1 658 ± 188.2 SVs/s of $Myo6^{C442Y/C442Y}$ mice, $n = 12$, $P < 0.05$), testifying that $Myo6^{C442Y}$ point mutation mature mice IHCs have comparative weak function of exocytosis.

DISCUSSION

MYO6 was one of the earliest deafness genes identified [14]. In cochlear hair cells it has been suggested that MYO6 could be involved in anchoring their apical membrane to the underlying actin-rich cuticular plate and also in the intracellular transport of synaptic vesicles and basolateral membrane proteins required for the functional maturation of IHCs at the onset of hearing [11, 15]. Mutations in the gene encoding myosin VI have been associated with dominant progressive and recessive congenital deafness in humans [7, 8]. The extraordinary sensitivity and timing accuracy of the auditory system depend on the exocytosis of the hair cell ribbon synapses, which work at the most appropriate frequency. Therefore, we comprehensively reveal the deafening mechanism of MYO6 mutation by analyzing the synaptic transmission function of inner hair cells on different mouse models systematically. In the present study, we studied ribbon synapse functions in immature and mature IHCs of both $Myo6^{-/-}$ and $Myo6^{C442Y/C442Y}$ mice, allowing us to compare and contrast MYO6 functions over different developmental stages and different mutants. Our study revealed the complexity of MYO6 functions in hearing, which is valuable towards building a whole and complete understanding of hearing deficits in DFNA22 and DFNB37.

It is reported that MYO6 exists in the active region of IHC synapses, and its absence prevents the normal maturation of IHC ribbon synapses [10]. We found that MYO6 deletion did not change the I_{Ca} amplitude of IHCs, but lead to a markedly reduced synaptic exocytosis of IHCs both in immature and mature mice (Figs. 1B, 2C, 3B and 4C). The role of MYO6 in IHCs exocytosis is consistent with several studies. Roux et al. found that compared with wild-type mice, the amplitude of Ca^{2+} currents on the IHCs of adult Snell's waltzer mutant mice has no obvious difference, but the vesicle release was significantly reduced [10]. MYO6 is necessary for efficient secretion and maintenance of Golgi apparatus structure [16]. This is also manifested in synaptic vesicle exocytosis of neuronal synapses [17]. In hippocampal neurons, both spontaneous and induced synaptic vesicle exocytosis were reduced by 35% in Snell's waltzer mice [18]. And studies have shown that the defect of Ca^{2+}- induced exocytosis is partial and only appears in mature IHCs absence of MYO6 [10], which consistent with our results (Figs. 2D and 4D). The reduced synaptic exocytosis observed in mature MYO6 knock-out mice IHCs may in principle be due to failure of IHC synaptic development, defective vesicle transport, inefficient Ca^{2+}- exocytosis coupling, or a combination of these defects. On the contrary, on the same Snell's waltzer mice model, the amplitude of Ca^{2+} currents in IHCs decreased, but there was no significant difference in vesicle release compared with wild-type mice [11].

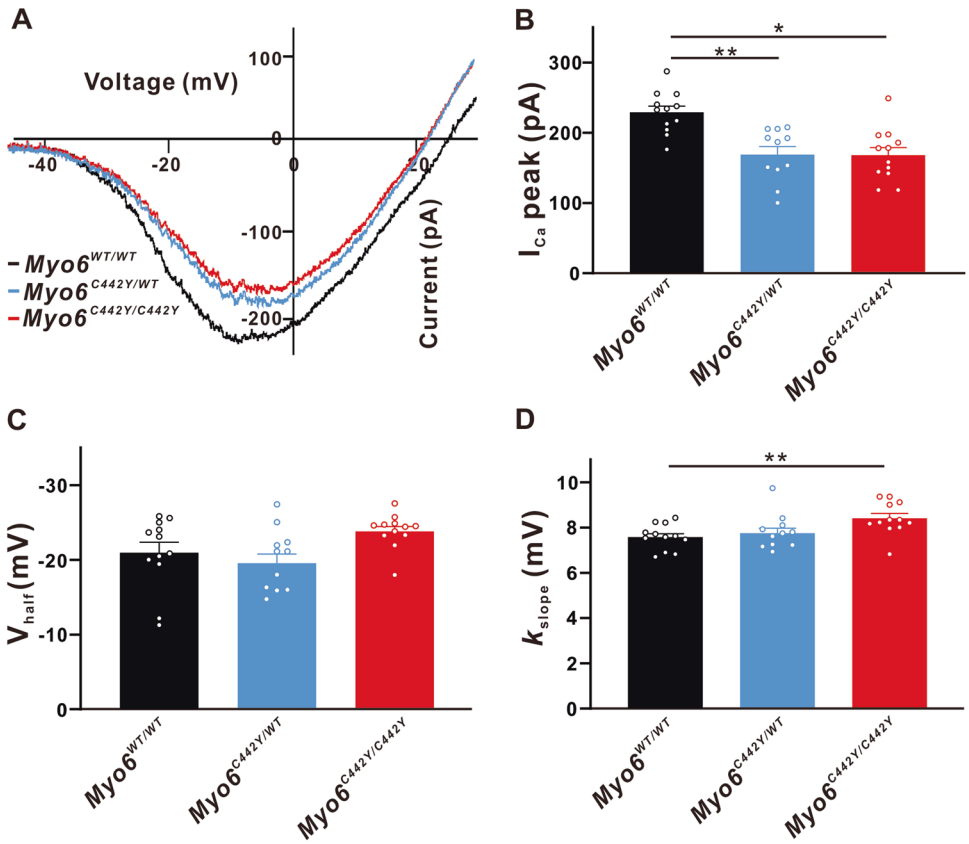

Fig. 7 Properties of I_{Ca} in mature IHCs. A Representative I-V curve of Ca^{2+} currents recorded from *Myo6*$^{WT/WT}$ mice (black), *Myo6*$^{C442Y/WT}$ mice (blue) and *Myo6*$^{C442Y/C442Y}$ mice (red) IHCs at P18-20. **B** *Myo6*^{C442Y} point mutation mice IHCs have smaller I_{Ca} amplitude than wild-type mice. **C**, **D** I_{Ca} in *Myo6*$^{C442Y/C442Y}$ mice IHCs has a similar V_{half} and a bigger k_{slope} compared to *Myo6*$^{WT/WT}$ mice. Data are presented as the mean ± SEM. Statistical analysis was by one-way ANOVA. * means $P < 0.05$ and ** means $P < 0.01$.

It is worth noticing that at least two kinetically distinct components of vesicle release were in mammalian hair cells: a rapidly small RRP and a slower but larger SRP, and RRP depletion is discussed as a mechanism for fast auditory adaptation. Our results indicated that both MYO6 knock-out developing mice and mature mice replenish synaptic vesicles less efficiently, which manifesting the poor function of exocytosis (Figs. 2E–G and 4E–G). The reason for these in the IHCs, the main source for IHCs synaptic vesicle pool replenishment is endocytosis at the synaptic active zone and the peri-cuticular necklace [19, 20]. And the abundance of MYO6 in these two regions, its association with tubular structures, likely endocytic structures and the protein is involved in endocytic membrane-trafficking together show that MYO6 is involved in the transport of actin-filament vesicles from the apical region of IHCs to ribbon synapses and/or the retrieval of IHCs synaptic vesicles after exocytosis [21–23]. Moreover, we found that I_{Ca} in Myo6$^{-/-}$ mature mice has a significantly negative V_{half} and a steeper k_{slope}, showing a hyperpolarizing tendency and stronger voltage-dependence in Ca^{2+} current activation which function synergistically to bring substantially more Ca^{2+} influx the cell under physiological conditions (Figs. 3C, D and 4B). Excessive calcium inflow can lead to an imbalance of Ca^{2+} homeostasis, thus activating a variety of kinases, destroying cytoskeleton and axons, causing energy metabolism and material metabolism disorders, eventually resulting in IHCs impaired, which is directly related to hearing loss [24, 25].

Unlike the MYO6 knock-out mice, the synaptic transmission function of the *Myo6*^{C442Y} point mutation developing mice has not significantly discrepancy compared with that of the wild-type. But we found that *Myo6*$^{C442Y/C442Y}$ mature mice has remarkably less Ca^{2+} influx the IHCs, down-regulation of ΔC_m and lower efficiency of Ca^{2+} triggering synaptic vesicles release for stimulation duration 500 ms. (Fig. 8B–D). Hearing depends on the faithful transmission of auditory signals from IHC to SGN through ribbon synapses [26]. At hair cell afferent synapses, a synaptic ribbon is affiliated with the sites of Ca^{2+} channel clustering and exocytosis. And voltage-gated Ca^{2+} channels are activated according to the graded membrane potential in IHCs and regulate the exocytosis of synaptic vesicles [27]. Changes in the number or characteristics of calcium channels may affect the release of synaptic vesicles of IHCs, which change the synaptic transmission function and eventually lead to hearing loss. Some studies provided clues indicating that vesicle pool replenishment is influenced by Ca^{2+} and depends on a Ca^{2+}-sensor protein unique to hair cells called otoferlin [28], which is roughly consistent with our results testifying that *Myo6*^{C442Y} point mutation mature mice IHCs have the comparative weak function of exocytosis. MYO6 is directly involved in cargo transport in many cell types [5], and it has been shown to be expressed in the basal pole of IHCs where ribbon synapses are located [10]. It is therefore likely that MYO6 is involved in the maturation, recycling and priming of vesicles. Specifically, Cys^{442} is located at the end of an α-helix that connects the nucleotide-binding structure [29], so that it is not surprising that a mutation at this site change the cargo transport speed of MYO6, ultimately affecting exocytosis at ribbon synapses.

In conclusion, our results suggest that compared with wild-type mice, the ribbon synaptic transmission function of IHCs from different Myosin VI mutant mice is down-regulated, further revealing the physiological and pathological mechanism of Myosin VI in hearing and deafness.

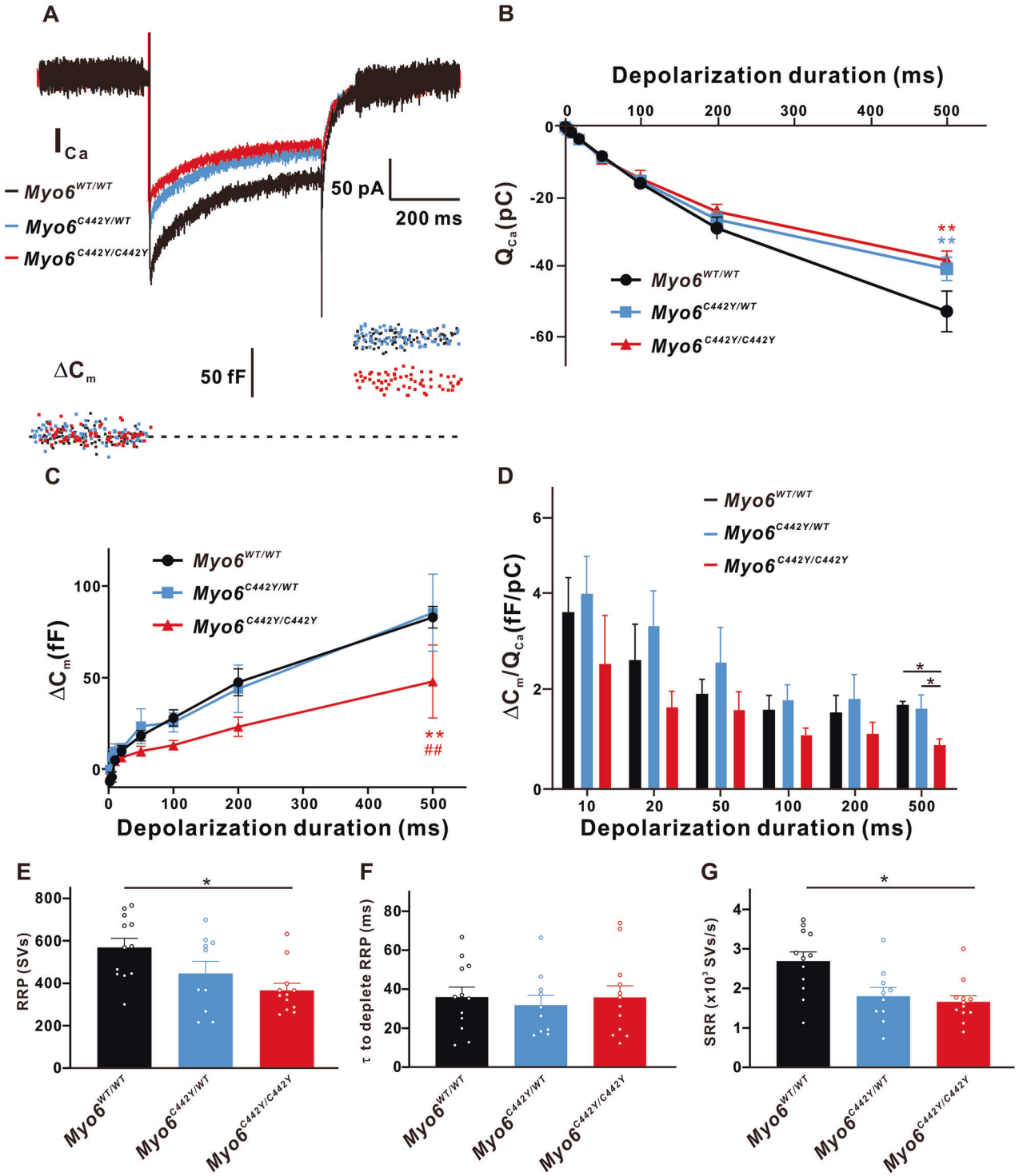

Fig. 8 Exocytosis from mature IHCs. A A representative diagram of I_{Ca} and the corresponding ΔC_m in $Myo6^{WT/WT}$ mice (black), $Myo6^{C442Y/WT}$ mice (blue) and $Myo6^{C442Y/C442Y}$ mice (red) IHCs at P18-20 of stimulation duration 500 ms. **B** Q_{Ca} in $Myo6^{C44Y2/WT}$ and $Myo6^{C442Y/C442Y}$ mice IHCs are significant difference than that of $Myo6^{WT/WT}$ mice for duration 500 ms. **C**, **D** ΔC_m (**C**) and the ratio of $\Delta C_m/Q_{Ca}$ (**D**) recorded from $Myo6^{C442Y/C442Y}$ mice IHCs are remarkable down-regulation than that from $Myo6^{WT/WT}$ and $Myo6^{C44Y2/WT}$ mice of duration 500 ms. **E**–**G** RRP (E) and SRR (**G**) from $Myo6^{C442Y/C442Y}$ mice IHCs are obviously smaller than that from $Myo6^{WT/WT}$ mice IHCs, but there is no distinct change inτto deplete RRP from three genotypes mature mice IHCs. Data are presented as the mean ± SEM. Statistical analysis was by one-way or two-way ANOVA. * means $P < 0.05$, ** means $P < 0.01$, ## means $P < 0.01$.

MATERIALS AND METHODS

Animals

All experimental procedures described here met the National Institutes of Health guidelines for the Care and Use of Laboratory Animals and were approved by the animal care committee of Fudan University. All mice (both male and female), both developing (age of 8 ~ 10 days) and mature (age of 18 ~ 20 days) were housed on a 12-h light/dark cycle with standard food and water provided ad libitum. We tried our best to minimize the number of animals and their suffering during this study. Sample size and inclusion/exclusion criteria were determined based on previous studies and the

results of this study. And no randomization and blinding were used to determine how animals were allocated to experimental groups and processed.

Myo6$^{C442Y/WT}$, *Myo6*$^{C442Y/C442Y}$ and *Myo6*$^{WT/WT}$ (control) mice were established by Beijing Biocytogen. Cas9 mRNA and sgRNA were microinjected into fertilized C57BL/6 J oocytes together with a targeting vector containing the C442Y allele to generate F0 founders. Myo6-C442Y mice were crossed with CBA/CaJ mice. Choose progenies without Cdh23ahl, because C57BL/6 J mice have age-related hearing loss due to homozygous Cdh23ahl alleles. Male and female Myo6-C442Y heterozygous mice were crossed to breed WT, heterozygous and homozygous offspring.

Myo6$^{+/-}$, *Myo6*$^{-/-}$ and *Myo6*$^{WT/WT}$ (control) mice were prepared using the EGE system developed by Biocytogen based on CRISPR/Cas9. By analyzing the structure of EGE-GJ-033 gene, Exon5 can be knocked out. The sgRNAs were designed in the nonconservative regions of Intron4 and Intron5, respectively, so as to achieve the goal of EGE-GJ-033 gene knockout.

Electrophysiological recordings

Recordings were achieved at room temperature (20–25 °C). To examine the function of inner hair cells, membrane currents and membrane capacitance (Cm) of IHCs from the apical turn of the sensory epithelium were recorded by conventional whole-cell patch-clamp techniques. Observe the IHCs through a 60×water-immersion objective on the Olympus microscope, and use an EPC10/2 amplifier (HEKA Electronics, Lambrecht Pfalz, Germany) driven by the Patchmaster software (HEKA Electronics) executing patch-clamp recordings. The hair cells were held at −90 mV (millivolt). The liquid junction potential of −10 mV was corrected offline and data were corrected subtracting 10 mV from all potentials.

The apical turns of cochlea were bathed in an oxygenated extracellular solution containing (in mM): 125 NaCl, 10 HEPES, 5.8 KCl, 5.6 D-glucose, 5 $CaCl_2$, 0.9 $MgCl_2$, 0.7 $NaH_2PO_4{\cdot}H_2O$, and 2 Na-pyruvate, pH 7.2 adjusted with NaOH, 300 mOsm/L with NaCl. Patch pipettes coated with dental wax had resistance of 5–6 MΩ full of internal solutions containing (in mM): 135 Cs-methane sulfonate, 10 CsCl, 10 TEA-Cl, 10 HEPES, 3 Mg-ATP, 2 EGTA and 0.5 Na-GTP, pH 7.2 adjusted with NaOH, 290 mOsm/L.

To record Ca^{2+} currents, we applied a slow-rising ramp voltage stimulation from −90 mV to +70 mV to induce whole-cell Ca^{2+} currents, and the peak of this Ca^{2+} currents (I_{Ca}) was determined. And recording whole-cell Ca^{2+} currents under different voltages obtained the current-voltage curve (I-V curve) and fitted to the Boltzmann equation:

$$I(V) = \left(V - V_{eq}\right) \cdot \frac{G_{max}}{1 + \exp\left(-\left(V - V_{1/2}\right)/k\right)}$$

half-activation voltage (V_{half}) and the slope factor (k) reflecting the steepness of voltage dependence in Ca^{2+} currents activation were obtained from different cells, averaged within the group, and then statistically compared between groups.

In order to quantify the synaptic vesicle release on IHCs, we will apply voltage stimulation to induce the vesicle release, and set a small sine wave voltage stimulation before and after the voltage stimulation. The whole cell membrane capacitance (C_m) can be measured according to the current response of the cell passive membrane characteristics to sine wave voltage stimulation, and the change of the C_m before and after stimulation can measure the exocytosis of synaptic vesicles from IHCs. We fixed the stimulation voltage at −10 mV, and applied 2, 5, 10, 20, 50, 100, 200 and 500 ms (millisecond) to obtain the vesicle release-time data (ΔC_m-t curve). Then we will use the simple exponential and linear mixed equation [30]:

$$\Delta C_m(t) = C_{m,RRP} \cdot \left(1 - \exp\left(\frac{t}{\tau_{RRP}}\right)\right) + R_{sustained} \cdot t$$

a single exponential function for release of readily releasable pool (RRP) of synaptic vesicles ($C_{m,RRP}$, τ_{RRP}) and a linear function for sustained release of synaptic vesicles ($R_{sustained}$). Then the numbers of synaptic vesicles were estimated with the capacitance values, using a conversion factor of 37 aF/vesicle [19].

Data analysis

Data analysis was performed using Igor 4.0 software (WaveMetrics, Lake Oswego, OR, USA) and GraphPad Prism software 5.0 (GraphPad Software, La Jolla, CA). The data meet the normal distribution. And the variances between the groups being statistically compared are similar. Data are presented as mean ± SEM. Apply one-way and two-way ANOVA with Bonferroni's post-hoc test (multiple comparisons). *P* value less than 0.05 was deemed significant.

DATA AVAILABILITY

The datasets used and/or analyzed during the current study are available from the corresponding author on reasonable request.

REFERENCES

1. Schrijver I, Gardner P. Hereditary sensorineural hearing loss: advances in molecular genetics and mutation analysis. Expert Rev Mol Diagn. 2006;6:375–86.
2. DiStefano MT, Hemphill SE, Oza AM, Siegert RK, Grant AR, Hughes MY, et al. ClinGen expert clinical validity curation of 164 hearing loss gene-disease pairs. Genet Med. 2019;21:2239–47.
3. Friedman TB, Belyantseva IA, Frolenkov GI. Myosins and Hearing. Adv Exp Med Biol. 2020;1239:317–30.
4. Roux I, Safieddine S, Nouvian R, Grati M, Simmler MC, Bahloul A, et al. Otoferlin, defective in a human deafness form, is essential for exocytosis at the auditory ribbon synapse. Cell. 2006;127:277–89.
5. Batters C, Veigel C. Mechanics and Activation of Unconventional Myosins. Traffic. 2016;17:860–71.
6. Weiss A, Schiaffino S, Leinwand LA. Comparative sequence analysis of the complete human sarcomeric myosin heavy chain family: implications for functional diversity. J Mol Biol. 1999;290:61–75.
7. Ahmed ZM, Morell RJ, Riazuddin S, Gropman A, Shaukat S, Ahmad MM, et al. Mutations of MYO6 are associated with recessive deafness, DFNB37. Am J Hum Genet. 2003;72:1315–22.
8. Melchionda S, Ahituv N, Bisceglia L, Sobe T, Glaser F, Rabionet R, et al. MYO6, the human homologue of the gene responsible for deafness in Snell's waltzer mice, is mutated in autosomal dominant nonsyndromic hearing loss. Am J Hum Genet. 2001;69:635–40.
9. Deol MS, Green MC. Snell's waltzer, a new mutation affecting behaviour and the inner ear in the mouse. Genet Res. 1966;8:339–45.
10. Roux I, Hosis S, Johnson SL, Bahloul A, Cayet N, Nouaille S, et al. Myosin VI is required for the proper maturation and function of inner hair cell ribbon synapses. Hum Mol Genet. 2009;18:4615–28.
11. Heidrych P, Zimmermann U, Kuhn S, Franz C, Engel J, Duncker SV, et al. Otoferlin interacts with myosin VI: implications for maintenance of the basolateral synaptic structure of the inner hair cell. Hum Mol Genet. 2009;18:2779–90.
12. Wang JH, Shen J, Guo L, Cheng C, Chai RJ, Shu YL, et al. A humanized mouse model, demonstrating progressive hearing loss caused by MYO6 p.C442Y, is inherited in a semi-dominant pattern. Hear Res. 2019;379:79–88.
13. Moser T, Beutner D. Kinetics of exocytosis and endocytosis at the cochlear inner hair cell afferent synapse of the mouse. Proc Natl Acad Sci USA. 2000;97:883–8.
14. Avraham KB, Hasson T, Steel KP, Kingsley DM, Russell LB, Mooseker MS, et al. The mouse Snell's waltzer deafness gene encodes an unconventional myosin required for structural integrity of inner ear hair cells. Nat Genet. 1995;11:369–75.
15. Hertzano R, Shalit E, Rzadzinska AK, Dror AA, Song L, Ron U, et al. A Myo6 mutation destroys coordination between the myosin heads, revealing new functions of myosin VI in the stereocilia of mammalian inner ear hair cells. PLoS Genet. 2008;4:e1000207.
16. Buss F, Arden SD, Lindsay M, Luzio JP, Kendrick-Jones J. Myosin VI isoform localized to clathrin-coated vesicles with a role in clathrin-mediated endocytosis. EMBO J. 2001;20:3676–84.
17. Osterweil E, Wells DG, Mooseker MS. A role for myosin VI in postsynaptic structure and glutamate receptor endocytosis. J Cell Biol. 2005;168:329–38.
18. Yano H, Ninan I, Zhang H, Milner TA, Arancio O, Chao MV. BDNF-mediated neurotransmission relies upon a myosin VI motor complex. Nat Neurosci. 2006;9:1009–18.
19. Lenzi D, Runyeon JW, Crum J, Ellisman MH, Roberts WM. Synaptic vesicle populations in saccular hair cells reconstructed by electron tomography. J Neurosci. 1999;19:119–32.
20. Griesinger CB, Richards CD, Ashmore JF. Fast vesicle replenishment allows indefatigable signalling at the first auditory synapse. Nature. 2005;435:212–5.
21. Cingolani LA, Goda Y. Actin in action: the interplay between the actin cytoskeleton and synaptic efficacy. Nat Rev Neurosci. 2008;9:344–56.
22. Toomre D, Keller P, White J, Olivo JC, Simons K. Dual-color visualization of trans-Golgi network to plasma membrane traffic along microtubules in living cells. J Cell Sci. 1999;112:21–33.
23. Kreitzer G, Marmorstein A, Okamoto P, Vallee R, Rodriguez-Boulan E. Kinesin and dynamin are required for post-Golgi transport of a plasma-membrane protein. Nat Cell Biol. 2000;2:125–7.

24. Verkhratsky A, Toescu EC. Calcium and neuronal ageing. Trends Neurosci. 1998;21:2–7.
25. Bredesen DE, Rao RV, Mehlen P. Cell death in the nervous system. Nature. 2006;443:796–802.
26. Wichmann C, Moser T. Relating structure and function of inner hair cell ribbon synapses. Cell Tissue Res. 2015;361:95–114.
27. Frank T, Rutherford MA, Strenzke N, Neef A, Pangršič T, Khimich D, et al. Bassoon and the synaptic ribbon organize Ca^2+ channels and vesicles to add release sites and promote refilling. Neuron. 2010;68:724–38.
28. Pangrsic T, Lasarow L, Reuter K, Takago H, Schwander M, Riedel D, et al. Hearing requires otoferlin-dependent efficient replenishment of synaptic vesicles in hair cells. Nat Neurosci. 2010;13:869–76.
29. Rayment I, Rypniewski WR, Schmidt-Base K, Smith R, Tomchick DR, Benning MM, et al. Three-dimensional structure of myosin subfragment-1: A molecular motor. Science. 1993;261:50–58.
30. Johnson SL, Franz C, Knipper M, Marcotti W. Functional maturation of the exocytotic machinery at gerbil hair cell ribbon synapses. J Physiol. 2009;587:1715–26.

ACKNOWLEDGEMENTS

None.

AUTHOR CONTRIBUTIONS

NY concept and design, literature search, experimental studies, data acquisition, data analysis, statistical analysis, manuscript preparation; JZ literature search, software, experimental studies, data analysis, statistical analysis; PZ experimental studies, data analysis, statistical analysis; BY data analysis, manuscript editing and manuscript review; RC concept and design, supervision, manuscript editing and manuscript review; G-LL concept and design, supervision, manuscript editing and manuscript review, resources support.

FUNDING

This work was supported by three grants to G.-L. Li from the National Natural Science Foundation of China (82171141), the Ministry of Science and Technology of China (2021YFA1101302), and the Science and Technology Commission of Shanghai Municipality (21JC1401000).

COMPETING INTERESTS

The authors declare that they have no known competing financial interests or personal relationships that could have appeared to influence the work reported in this paper.

ETHICS

All experimental procedures described here met the National Institutes of Health guidelines for the Care and Use of Laboratory Animals and were approved by the animal care committee of Fudan University.

ADDITIONAL INFORMATION

Correspondence and requests for materials should be addressed to Renjie Chai or Geng-Lin Li.

Reprints and permission information is available at http://www.nature.com/reprints

Publisher's note Springer Nature remains neutral with regard to jurisdictional claims in published maps and institutional affiliations.